

A study on PIV-based pressure measurements using CFD techniques

F. Felis-Carrasco¹, B. B. Watz¹, D. Hess^{1*}, M. A. Mendez²

¹ Dantec Dynamics A/S/Company, Copenhagen, Denmark

² von Karman Institute for Fluid Dynamics, Sint-Genesius-Rode, Belgium

* dhs@dantecdynamics.com

Abstract

This work discusses an approach to compute pressure fields from planar PIV measurement using standard CFD tools. In particular, we propose a combination of interpolation and mesh adaptation to import the PIV measurements on a grid that is morphed around objects, and is fine enough to solve the Poisson equation accurately. The whole process of meshing, interpolation and pressure computation is carried out using the popular open-source solver OpenFoam®. The method is tested and validated on a classic benchmark test case, namely, the unsteady flow past a cylinder. A 3D multiphase flow simulation is used to generate the reference data and analyze the impact of both, the PIV interrogation and the interpolation on the morphed grid. The simulation uses an Euler-Lagrangian one-way coupling approach to simulate the flow field and the dynamics of seeding particles. The analysis compares the pressure field from the 3D CFD simulation with the solution of a 2D Poisson equation based on the 2D velocity field obtained by either down-sampling the CFD data or by PIV interrogation of synthetic images built from the CFD data. Finally, we challenge the proposed method with the pressure reconstruction in a TR-PIV experiment in similar conditions.

1 Introduction

Measuring the flow field by planar or volumetric PIV is often the first step towards the solution of many aerodynamics, acoustics, and fluid-structure interaction problems. Phenomena such as boundary layer separation or travelling vortices can be identified within the measurement domain and linked to noise emission or aerodynamic loads. Further insights on many of these phenomena are possible if the pressure fields can be retrieved from the measurement domain. For example, aerodynamic loads, force balances and momentum exchanges can be evaluated by integrating pressure distributions along boundaries. Jakobsen et al. (1997) were among the first to estimate forces from PIV flow fields; since then, many approaches have been presented (see, van Oudheusden, 2013).

Regardless of the required input (either averaged fields or time-resolved sequences of instantaneous fields), most methods are based on the integration of a Poisson equation, derived from the momentum and mass conservation equations (see also, van Gent et al., 2017; van Oudheusden, 2013).

Standard techniques from CFD (Computational Fluid Dynamics) offers powerful and efficient tools to compute pressure fields from velocity fields (Gunaydinoglu and Kurtulus, 2020; Regert et al., 2011). However, the main challenge in the use of these tools is that PIV fields are generally noisy and available on grids that are often too coarse to reproduce accurately curved boundaries. Adaptive PIV interrogation methods (see for example, Masullo and Theunissen (2017)) offer a valuable solution but are not yet widely diffused.

In this work, we propose a combination of interpolation and mesh adaptation to compute pressure fields from planar PIV using the popular open-source CFD package OpenFOAM®. In particular, we analyze the impact of the interpolation and mesh adaptation and the PIV interrogation by testing the algorithm on a test case, for which the ground truth is available. The selected test case is the unsteady flow past a cylinder, which was first simulated using a 3D Euler-Lagrangian simulation. This allows reproducing the flow field and the seeding particle dynamics. Besides providing the reference data, the CFD results were also used to extract a set of 2D fields on grid step sizes similar for PIV and reproduce a set of synthetic PIV images. The

first was used to analyze the impact of the velocity field interpolation; the second was used to analyze the impact of the PIV interrogation area size.

The numerical methods are discussed in Section 2 while Section 3 presents the test case and the related computation. Finally, we close in Section 4 with an assessment of the method on Time-Resolved PIV experiment in a similar configuration, where the additional challenge of a limited region of interest and unknown boundary conditions are included. Conclusions and perspectives are given in Section 5.

2 Numerical method for pressure calculation

The starting point for the pressure calculation is the set of mass and momentum conservation equations. Considering an incompressible flow with constant density ρ and constant kinematic viscosity ν , the continuity equation imposes the divergence-free (solenoidal) condition to the velocity field. In Cartesian coordinates, denoting the velocity components as u_i with $i = 1, 2, 3$, and using Einstein notation, this reads $\partial u_i / \partial x_i = 0$. With the same notation, the momentum conservation equations read:

$$\frac{\partial u_i}{\partial t} + \frac{\partial u_i u_j}{\partial x_j} = -\frac{\partial p}{\partial x_i} + \frac{\partial}{\partial x_j} \left[\nu \left(\frac{\partial u_i}{\partial x_j} + \frac{\partial u_j}{\partial x_i} - \frac{2}{3} \frac{\partial u_k}{\partial x_k} \delta_{ij} \right) \right], \quad (1)$$

where p is here the kinematic pressure (i.e. P/ρ , with P the static pressure). The link between the velocity field and the pressure field is given by the Poisson equation obtained by taking the divergence of (1):

$$\frac{\partial^2 P}{\partial x_i^2} = \underbrace{\frac{\partial}{\partial x_i} \left[\frac{\partial u_i}{\partial t} \right]}_{\text{time source}} + \underbrace{\frac{\partial}{\partial x_i} \left[\frac{\partial u_i u_j}{\partial x_j} \right]}_{\text{convective source}} + \underbrace{\frac{\partial}{\partial x_i} \left[\frac{\partial}{\partial x_j} \nu \left(\frac{\partial u_i}{\partial x_j} + \frac{\partial u_j}{\partial x_i} - \frac{2}{3} \frac{\partial u_k}{\partial x_k} \delta_{ij} \right) \right]}_{\text{diffusive source}}. \quad (2)$$

In its general form, this equation includes three source terms on the right hand side. The first is related to the flow unsteadiness, the second to the advection term and the last to the viscous diffusion. The divergence-free condition from the continuity equation significantly simplifies this equation. However, when working with 2D measurements, the assumption of solenoidal 2D fields implies that the out-of plane component is identically null and is thus an important source of errors.

2.1 Numerical solver in OpenFOAM®

An integration scheme and adequate boundary conditions are needed to solve the Poisson Eq. (2) for the pressure. Many approaches have been explored over the years, from direct integration using finite differences methods to complete implementations of CFD solvers like *SIMPLE* or *PISO*, where both the pressure and the velocity fields are calculated and corrected in an iterative process (Gunaydinoglu and Kurtulus, 2020; Regert et al., 2011).

A direct approach is used in this work, namely a standard Poisson solver using Finite-Volume Method (FVM) from OpenFOAM®. In this solver, the velocity field u_i and hence all terms on the right hand side of Eq. (2) are assumed to be known. The solver was implemented in a custom solver inherited from a *PISO* solver from the OpenFOAM® tools. Within this, a GAMG (Geometric Algebraic Multi-Grid) solver is applied, with a maximum of 10 non-orthogonal correction steps, until a residual of $1e-9$ is reached.

The boundary conditions consist of a mixture of Dirichlet and Neumann conditions. Dirichlet conditions $p = 0$ are set to all ‘open’ boundaries of the domain that are sufficiently far from the solid walls (e.g. the cylinder surface). The classic zero gradient $\partial p / \partial n$ along the normal direction n is imposed at solid walls. A different approach consists of using the velocity field along a boundary to compute the pressure gradient from Eq. (1), and finally set Neumann conditions accordingly. Nevertheless, this approach was not implemented in this study.

The pseudo-code to solve eq. (2) is detailed in the Appendix List. 1, where the step-by-step construction for the know source terms is shown using FVM classes in OpenFOAM® (OpenCFD-Limited, 2019a). From a syntax point-of-view, the same steps are taken when moving from Eq. (1) into Eq. (2).

2.2 Mesh Adaptation via Snappy Hex Mesh

The main challenge in computing the pressure field past a curved object is that standard PIV interrogation provides the flow field u_i on a coarse grid. Usually, this grid is not capable of representing a curved surface as the cylinder in the proposed test case.

In this work, we test the *snappyHexMesh* utility from OpenFOAM® to construct a mesh that conforms to the curved boundary. This utility uses hexahedra and split-hexahedra mesh elements which are iteratively refined and morphed to the curved surface (OpenCFD-Limited, 2019b). The process begins with a structured mesh which acts as a ‘background mesh’ and defines both the domain and the base level of mesh density. This is typically generated using the *blockMesh* utility. In the PIV-based pressure computation, the background mesh is provided by the PIV grid.

The main steps are illustrated in Figure 1, using a down-sampled version of the CFD results to mimic the PIV field as discussed in Section 3. Figure 1-a shows the initial coarse mesh and the expected pressure field, while Figure 1-b shows the velocity fields interpolated on the morphed mesh. Note that the original grid in Figure 1-a is incapable of describing the cylinder surface. Figure 1-c shows the adapted mesh and the results the solution of the Poisson equation together with the velocity field interpolation. Finally, once the solution for the pressure is found in the adapted mesh, the result is interpolated back into the original PIV grid. The results are shown in Figure 1-d, which is to be compared, as discussed in Section 3, with Figure 1-a.

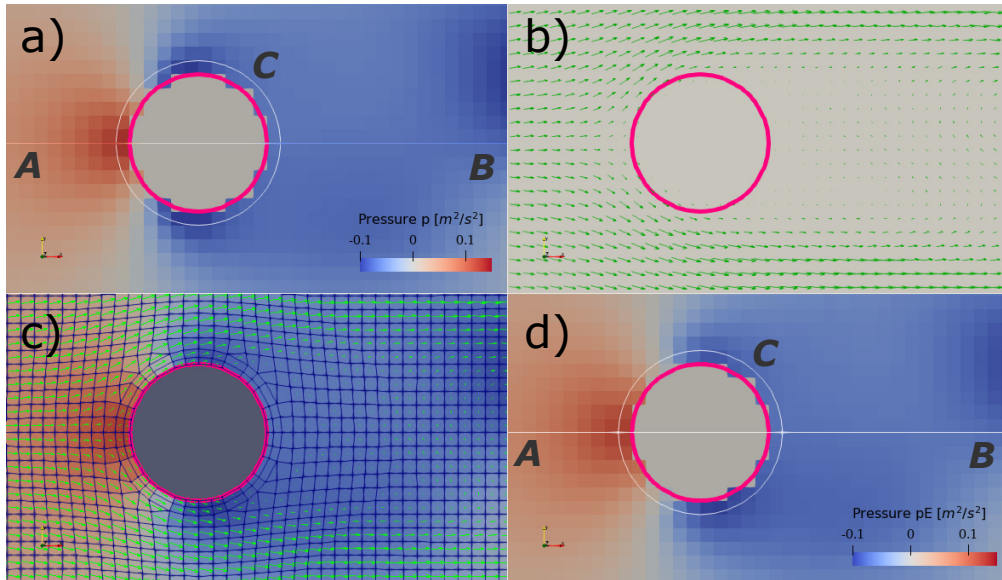


Figure 1: Steps for the mesh adaptation and pressure computation around an object. For validation purposes, as described in Sec. 3, Figure a) shows the pressure field available over a coarse grid. Figure b) shows the 2D velocity vector field (green arrows) interpolated from the original downsampled 3D CFD simulation. Figure c) shows the morphed mesh around a re-inserted cylinder object together with the pressure solution (pE) from the solver. Figure d) shows the interpolation of the result back to the original coarse grid.

3 Case study for proof-of-concept: flow past a cylinder

The procedure to validate the proposed methodology is illustrated in Figure 2. The CFD simulation, described in Section 3.1, allows for controlled numerical experiments in which both velocity and pressure fields are available on a fine grid and in a large domain. The CFD results are used for two purposes.

First, a coarse velocity vector field is extracted by down-sampling the 3D CFD results along with a 2D coarse mesh that mimics a PIV grid (grey boxes in Figure 2). This is used to re-compute the pressure fields using the Poisson solver described in the previous section. Details of these computations are reported in Section 3.2. This test case provides the “best-case” scenario for the solver (orange boxes in Figure 2) and allows evaluating the impact of the 2D assumption.

Second, the results from the Lagrangian tracking are used to generate synthetic 2D-2C PIV images. These are then processed using standard PIV interrogation algorithms, and the resulting velocity fields are also used to calculate the pressure field (blue boxes in Figure 2). Details of these computations are reported in Section 3.3. This test case allows for testing the impact of the PIV interrogation. Finally, Section 3.4 reports on the results of this comparison.

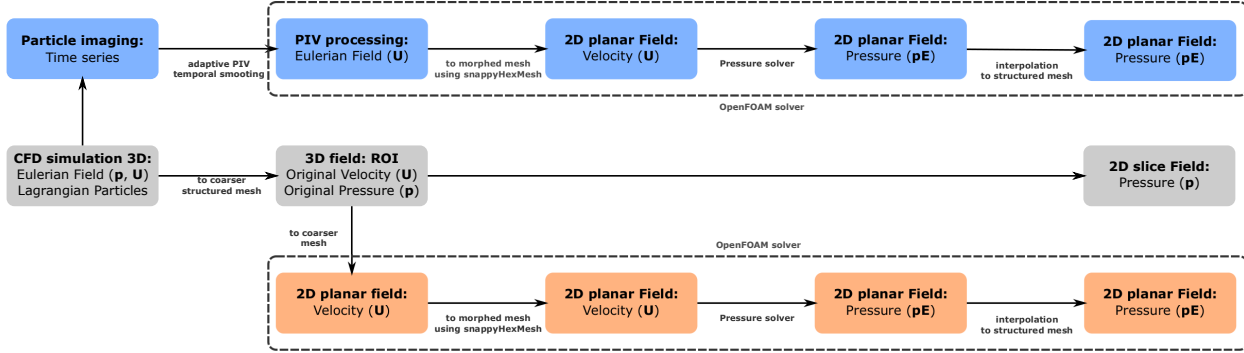


Figure 2: Flowchart of the proposed study case. The boxes in gray show the steps to obtain the reference data from the 3D transient CFD simulation. The boxes in orange show the steps to extract 2D pressure planes from the 3D data. The boxes in blue trace the step to obtain PIV based pressure evaluation from the CFD data, using synthetic images.

3.1 3D transient Euler-Lagrange simulation

The simulation case consist on a 3D transient flow around a fixed cylinder. The domain is a box of $[-50, 200]$ mm in the x direction, $[-50, 50]$ mm in the y direction and $[-125, 125]$ mm in the z direction. The cylinder is centered at the origin $(0, 0, 0)$ and oriented in the z direction, with a diameter $d_c = 5$ mm and a length of $L_c = 30d_c$. A snapshot of the 3D domain, illustrating also the mesh refinement along the middle plane $z = 0$ is shown in Figure 3-a.

The inlet free stream velocity is set to $u_\infty = 0.5$ m/s at the inlet plane $x = 0$. The fluid properties for air are taken as $\rho = 1.2047$ kg/m³ and $\nu = 15.11 \times 10^{-6}$ m²/s, leading to a diameter-referenced Reynolds number of $Re = u_\infty d / \nu = 170$. The flow is thus in the laminar unsteady regime.

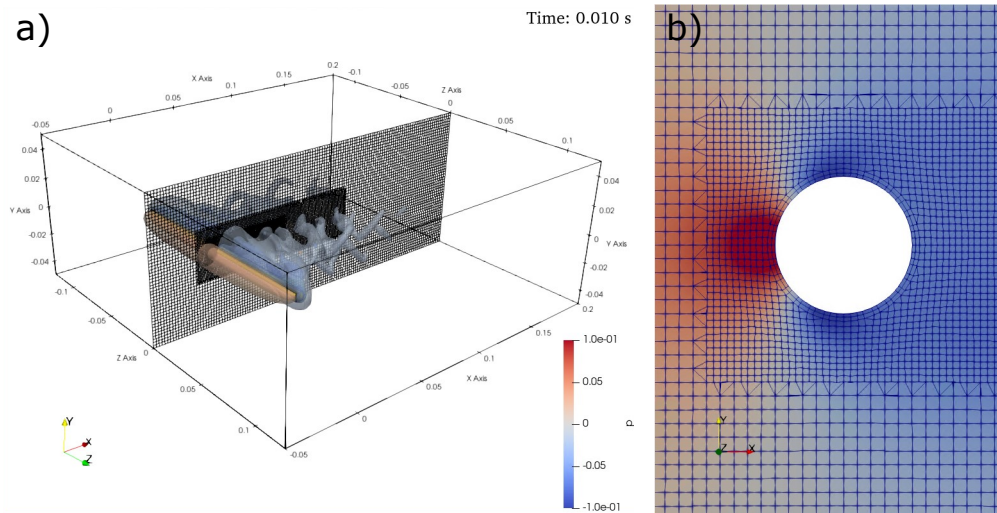


Figure 3: 3D transient CFD Euler/Lagrange simulation of the flow past a cylinder. Fig a) shows the calculation domain 3D iso-contours pressure surfaces around the cylinder. Fig b) shows a slice in the center plane of a), showing the mesh grading towards the 3D cylinder.

The iso-contours pressure surfaces in Figure 3-a indicate that the flow has a complex 3D topology downstream the cylinder, where the effect of the edges develops, reaching the center-plane ($z = 0$) for $x/d_c > 5$. Figure 3 shows a snapshot of the pressure field and the mesh refinements close to the cylinder.

The simulation is enriched with Lagrangian tracking of particle tracers in the Eulerian Fields. As described in Figure 2, these provides the required information to build synthetic PIV fields and assess the complete chain.

The Lagrangian solver uses a one-way coupling, meaning that the particles move according to the Eulerian field, but these do not alter the main flow. The simulations are carried out using the *uncoupledKinematicParcelFoam* in OpenFOAM®. A total of $20 \times 10^6 s^{-1}$ particles are injected in the domain inlet with initial velocity equal to 5% of the local velocity. These are injected at randomly selected location and are assumed to be spherical and mono-dispersed with a diameter of $d_p = 1 \mu m$. The particle density is set equal to the fluid flow to let them follow the flow accurately. Their interaction with surfaces is set to rebound, taking a stiffness Young's module of 6×10^6 Pa. Particles leaving the domain are set to disappear.

In both the 2D pressure field evaluation and the PIV-based reconstruction, the selected domain is taken as $-4 \leq x/d_c \leq 4$, namely in a region which is fairly bi-dimensional. To simulate a PIV experiment, the velocity field is assumed bi-dimensional, i.e. with $u_3 = 0$: regions in which this assumption is invalid produce out-of plane motion which cannot be quantified in a planar, single camera, PIV experiment. These invalidate the assumption of solenoidal 2D fields and prevents simplifications of Eq. (2).

3.2 Pressure Reconstruction from 2D Field

Following the work flow in the orange boxes of Figure 2, 2D fields simulating 2D-2C PIV measurements are obtained by under-sampling the 3D data on the plane $z = 0$. The original velocity field u_i and the pressure fields are linearly interpolated from the 3D grid onto a coarser regular 2D grid. In the process, we force $u_3 = 0$ to have 2D fields. However, we do not impose the condition of divergence free for the 2D flow u_1, u_2 and hence the Pressure Eq. (2), here solved in its 2D form, has the three source terms on the right hand side. However, it is worth noticing, that the region close to the cylinder ($-4 \leq x/d_c \leq 4$) is characterized by nearly solenoidal 2D fields.

The results were shown in Figure 1-a and 1-b. Given the position and the diameter of the cylinder, this is introduced in the flow field (red circle in Figure 1-a) in order to recreate a surface patch for the CFD calculation.

The *snappyHexMesh* utility is used to morph and adapt the original regular background grid into a grid capable of well representing the cylinder and the associated boundary conditions. The velocity field is then linearly interpolated again into this mesh, as shown in Figure 3-c. The Poisson solver described in Section 2 is used to compute the pressure field and the result is interpolated back into the original background mesh (Figure 3-d).

3.3 Pressure Reconstruction from PIV Measurements

The results from the Lagrangian tracking are used as input for a synthetic image generation engine. This procedure is based on the work of Lecordier and Westerweel (2004). The synthetic images with the size of 2400×1600 px represents a domain of $[-26, 52]$ mm in x direction and $[-26, 26]$ mm in y direction. The center of the cylinder is aligned with the $[0, 0]$ coordinate leaving 5-diameters upstream and 10 diameters downstream for the flow to develop.

The synthetic camera sensor has a $10 \mu m$ pixel size and is paired with a 100 mm lens positioned 325 mm away from the measurement plane. The particles are modelled with Gaussian intensity profiles with the size of 0.02 mm, resulting in a particle diameter of 2.4 px. The resulting seeding density is approximately 0.01 particles per pixel (ppp). PIV snapshots were generated with a frequency of 1000 Hz, imitating a TR-PIV acquisition in "single-exposure" mode. The PIV velocity fields are available at the same time instance of the simulation, which are sampled with twice the frequency.

The velocities from the particle images are computed in DynamicStudio using an Adaptive PIV algorithm (Theunissen, 2010) with a smallest size of 32×32 px using 50% overlap, resulting in a vector spacing of 0.48 mm. The vectors are filtered in time and space with a multiscale Proper Orthogonal Decomposition (mPOD) (Mendez et al., 2020) analysis and mPOD reconstruction with 98.5 % of the highest energetic modes. This is necessary since the velocities close to cylinder are more noisy, probably because of the lower seeding concentration in this area. Thereafter, the pressures are computed as in the previous section.

3.4 Analysis

Figure 4 shows the pressure profiles sampled along the circumference C and the line $A - B$ from Figure 1. The comparison along the circumference C is performed in a polar plot in which $\theta = 180^\circ$ is the front stagnation point and $\theta = 0^\circ$ is the rear stagnation point (see also Figure 1).

Four profiles are shown. Black continuous lines are used for the pressure profiles extracted from the 3D simulation. These can be considered as the ground truth. The profiles with the round blue markers are extracted from the down-sampled grid, onto which the pressure fields were interpolated. The excellent matching between these two curves shows that the morphed mesh is, in principle, well suited to reproduce the pressure fields in this configuration.

The profiles with the red round markers are obtained by integrating Eq. (2) on the coarse (PIV-live) grid, using the velocity available over it. The discrepancy is everywhere significant and is clearly because the grid is way too coarse. Besides introducing errors in the derivative computation, this grid is incapable of correctly describing the cylinder surface and does not allow, therefore, to set the boundary conditions of the problem correctly.

The results are significantly improved if Eq. (2) is solved over the morphed grid, with velocity fields linearly interpolated from the coarse mesh, as shown by the profiles with the orange square markers. This result is primarily due to the constraint of the no-slip condition on the cylinder, which helps the interpolation overcoming the limitations of linear support. Of course, more complex interpolations schemes might be needed for problems characterized by more significant gradients, but for the scopes of this work, the agreement is sufficient to prove the feasibility of the proposed approach. Moreover, these results highlight the importance of correctly defining the object geometry, both because of the required mesh refinement and because of the need to correctly impose the boundary conditions.

Finally, the profiles with green triangles are the ones obtained by integrating Eq. (2) over the morphed grid using velocity fields obtained via PIV interrogation. Although some discrepancies appear on the pressure profile along the line $A - B$ in the rear stagnation region, the agreement between the pressure distribution in the 2D pressure re-calculation and the PIV-based pressure evaluation is overall acceptable. This shows that the PIV evaluation, enhanced by the mPOD-based filter, provides fields that are sufficiently accurate. Additional mesh refinements, finer interrogation windows and/or better interpolation might be needed in the regions close to the boundary layer separation ($\theta \approx \pm 120^\circ$), in which the velocity gradients are more pronounced.

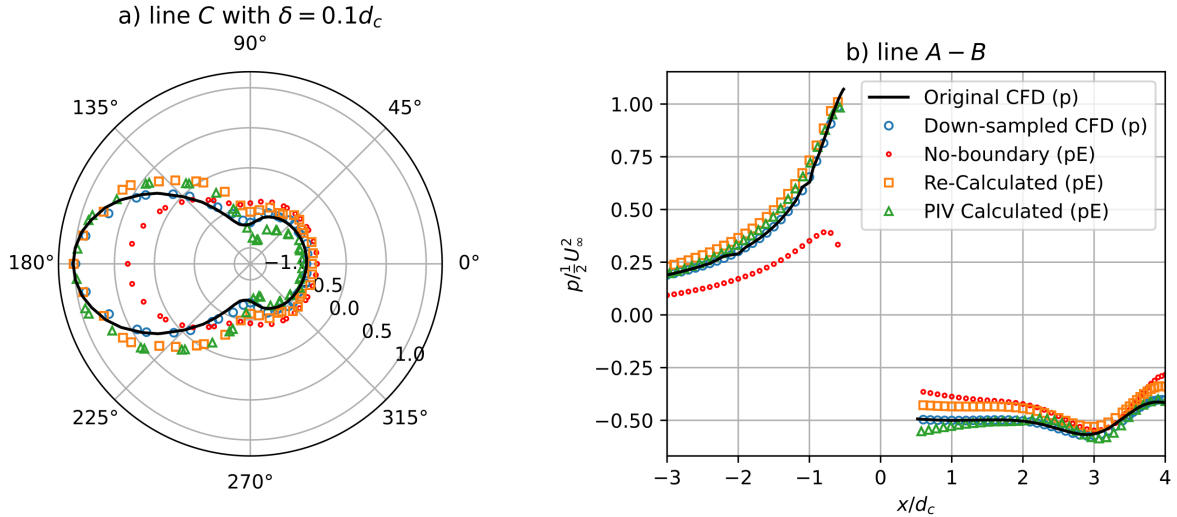


Figure 4: Comparison of the pressure field in the vicinity of the cylinder. a) Pressure around the cylinder object at $\delta = 0.1d_c$ from the surface. b) Pressure along the x axis centerline across the cylinder.

4 An Experimental Test Case

While the previous test cases allow for evaluating the impact of all the different steps in the pressure evaluation, we here consider an experimental test case. This is the time-resolved PIV measurement of the flow around a cylinder, using the same set set-up as the same used in Mendez et al. (2020).

The experiments are carried out in the L-10 low speed wind tunnel of the von Karman Institute. The tunnel offers a cross-section of 20 cm and the cylinder has a diameter of 5 mm. Seeding particles were injected in the intake manifold of the tunnel from a Laskin nozzle operated with Ondina Shell 91 mineral oil. These are illuminated by the Physics Instruments ND:YLF laser, offering up to 20 mJ/pulse at 1 kHz. The time resolved PIV system, from Dantec Dynamics, is completed by a SpeedSense 9090 camera running at 7200 Hz. DynamicStudio 7.3 is used for acquisition and analysis. The 1280×800 px camera with its 100 mm macro lens for this measurement has a pixel resolution of $50 \mu\text{m}/\text{px}$ and the total field of view is 64×40 mm.

The image interrogation was carried out using Adaptive PIV (Theunissen, 2010) with a final window size of 24×24 px and a vector spacing of 8 px, resulting in one vector every 0.4 mm. For temporal and spatial filtering a mPOD analysis and mPOD reconstruction with 97 % of the total energy is applied prior to the pressure computations. These 97 % of the total energy are represented by the 101 modes (including the mean) with the highest energy.

The free stream velocity is measured to $u_\infty = 1.25$ m/s resulting in a Reynolds number of $Re = 400$. With a vortex formation frequency of approximately $f = 48$ Hz, the Strouhal number is $St = fd/u_\infty = 0.192$. This is in the typical range for a vortex street behind a cylinder at the Reynolds number considered.

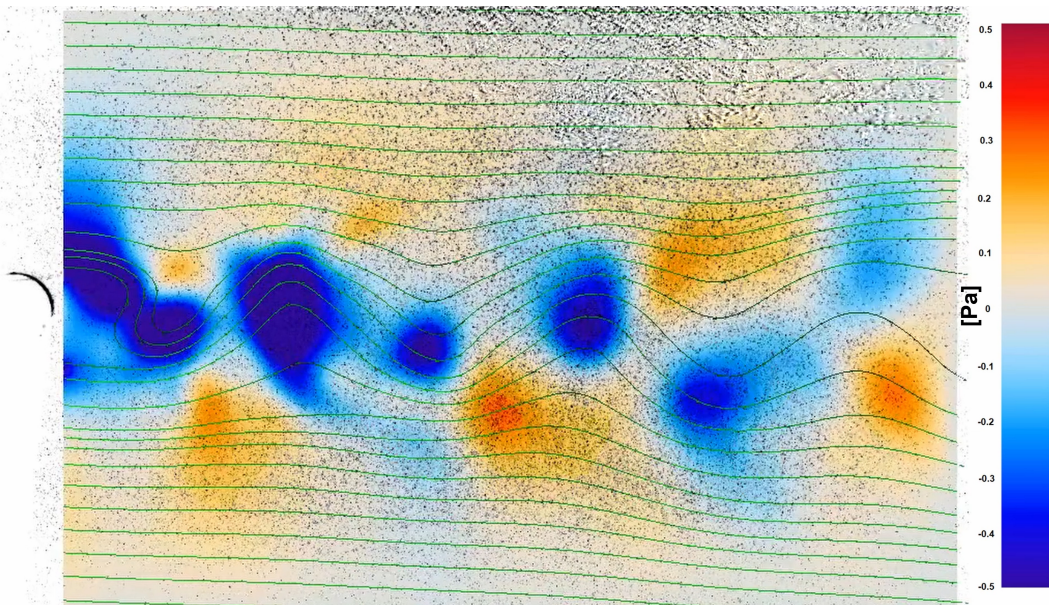


Figure 5: Result of the pressure computation from a conducted PIV experiment of a cylinder flow.

Unfortunately, this experimental test case was designed to focus on the wake dynamics and not on the flow in proximity of the cylinder. Because of a large shadow cast on the bottom side of the flow, the ROI for the PIV analysis can only be placed downstream the cylinder. The investigated ROI and the result from the pressure computation can be seen in Figure 5.

From these velocity fields, the pressures are computed using the explicit pressure computations using the methodology previously described. The main challenge here is the definition of the boundary conditions, particularly on the left edge of the ROI. In this first proof of concept, this was set to zero gradients, while zero pressure is set to all the other boundaries. These conditions on the left and right boundaries are not appropriate given the presence of non-negligible velocity gradients, and future studies will implement more sophisticated Neumann boundary conditions by reconstructing the pressure gradient from eq.(1) and the velocity close to the integration boundaries. Nevertheless, the results far from these boundaries appear realistic (with pressure minima correctly located at the centre of the vortices) and are therefore encouraging.

5 Conclusion and Perspectives

This work analyzed the implementation of a Poisson solver, using the popular CFD package OpenFOAM®, to compute pressure fields from 2D-2C PIV data.

The novelty of the approach lies in the treatment of objects immersed in the flow: by using the *snappy-HexMesh* routine from OpenFOAM®, an adapted mesh can be created around the object and refined starting from the PIV grid. The PIV field can then be interpolated on this grid.

The morphed mesh allows to better impose the no-slip boundary condition for the velocity and the zero-gradient for the pressure field, increasing the velocity interpolation and pressure integration accuracy.

A 3D transient multiphase simulation of a flow around a cylinder was used to benchmark the method and analyze the impact of the correct boundary definition, the interpolation and the PIV interrogation. In particular, the simulations reproduced both the flow field and the seeding distribution and was used for providing the reference data, for testing the impact of the velocity interpolation and the PIV interrogation, evaluated by reconstructing synthetic images from the CFD results. Among all the investigated factors, it appears that the correct definition of the curved wall plays the most important role: it allows for better reproducing the gradient of the flow and essential boundary conditions in the integration. Finally, a first implementation on an experimental data-set was presented, although better treatment of the boundary conditions is still to be implemented.

The proposed method could be further extended with (1) more advanced interpolation schemes (e.g. Radial Basis Functions), which potentially enable for additional constraints to the velocity interpolation, (2) by the use of more advanced PIV interrogation schemes to better resolve gradients along walls, which allows for better sample the flow and (3) by the use of an implicit solver that corrects the flow divergence while computing the pressures. These three research directions are currently being investigated.

Appendix

OpenFOAM C++ pseudo-code for the pressure solver implemented.

Listing 1: Pressure from PIV pseudo-code solver using OpenFOAM® tools.

```
// Momentum equation explicit terms (Vector Fields)
volVectorField ddtU("ddtU", rDeltaT*(U-Uold));
volVectorField divU("divU", fvc::div(phi, U));
volVectorField diffU(
    "diffU",
    fvc::div(turbulence->nu()*dev(twoSymm(fvc::grad(U))))
);

// Apply divergence and sign for Poisson equation (Scalar Fields)
volScalarField divDdtU("divDdtU", - fvc::div(ddtU));
volScalarField divDivU("divDivU", - fvc::div(divU));
volScalarField divDiffU("divDiffU", fvc::div(diffU));

// Poisson equation solution for pE
while (piso.correctNonOrthogonal())
{
    fvScalarMatrix pExpEqn
    (
        fvm::laplacian(pE) == divDdtU + divDivU + divDiffU
    );
    pExpEqn.setReference(pRefCell, pRefValue);
    pExpEqn.solve();
}
```

References

- Gunaydinoglu E and Kurtulus DF (2020) Pressure–velocity coupling algorithm-based pressure reconstruction from piv for laminar flows. *Experiments in Fluids* 61:1–20
- Jakobsen ML, Dewhirst TP, and Greated CA (1997) Particle image velocimetry for predictions of acceleration fields and force within fluid flows. *Measurement Science and Technology* 8:1502–1516
- Lecordier B and Westerweel J (2004) *The EUROPIV Synthetic Image Generator (S.I.G.) in: Particle Image Velocimetry: Recent Improvements*. Springer Berlin Heidelberg
- Masullo A and Theunissen R (2017) On the applicability of numerical image mapping for piv image analysis near curved interfaces. *Measurement Science and Technology* 28
- Mendez MA, Hess D, Watz BB, and Buchlin JM (2020) Multiscale proper orthogonal decomposition (mpod) of tr-piv data—a case study on stationary and transient cylinder wake flows. *Measurement Science and Technology* 31
- OpenCFD-Limited (2019a) Openfoam programmer’s guide version v1912
- OpenCFD-Limited (2019b) Openfoam user’s guide version v1912
- Regert T, Chatellier L, Tremblais B, and David L (2011) Determination of pressure fields from time-resolved data. in *9-th International Symposium on Particle Image Velocimetry*
- Theunissen R (2010) *Adaptive resolution in PIV image analysis - Application to complex flows and interfaces*. Doctoral Thesis von Karman Institute
- van Gent PL, Michaelis D, van Oudheusden BW, Weiss PE, de Kat R, Laskari A, Jeon YJ, David L, Schanz D, Huhn F, Gesemann S, Novara M, McPhaden C, Neeteson NJ, Rival DE, Schneiders JFG, and Schrijer FFJJ (2017) Comparative assessment of pressure field reconstructions from particle image velocimetry measurements and lagrangian particle tracking. *Experiments in Fluids* 58
- van Oudheusden BW (2013) Piv-based pressure measurement. *Measurement Science and Technology* 24:484–497